

Stability switching and hopf bifurcation in a two-delay predation system with diffusion and network coupling

Wenjie Yang(杨文杰), Jingxin Hu(胡静欣), Qianqian Zheng(郑前前), Jianwei Shen(申建伟), and Yiping Lin(林怡平)

Citation: Chin. Phys. B, 2026, 35 (**8**): 080204. DOI: 10.1088/1674-1056/ae5c8a
http://cpb.iphy.ac.cn; http://iopscience.iop.org/cpb

What follows is a list of articles you may be interested in

Hopf bifurcation and oscillatory dynamics in a delayed FitzHugh-Nagumo neuronal network on scale-free topologies

Zhan Shen(申瞻), Qianqian Zheng(郑前前), Jianwei Yang(杨建伟), and Jianwei Shen(申建伟)
Chin. Phys. B, 2026, 35 (**6**): 060202. DOI: 10.1088/1674-1056/ae594c

Sliding-mode-based preassigned-time control of a class of memristor chaotic systems

Jinrong Fan(樊金荣), Qiang Lai(赖强), Qiming Wang(汪其铭), and Leimin Wang(王雷敏)
Chin. Phys. B, 2024, 33 (**11**): 110205. DOI: 10.1088/1674-1056/ad7e9d

Mechanism analysis of regulating Turing instability and Hopf bifurcation of malware propagation in mobile wireless sensor networks

Xi-Xi Huang(黄习习), Min Xiao(肖敏), Leszek Rutkowski, Hai-Bo Bao(包海波), Xia Huang(黄霞), and Jin-De Cao(曹进德)
Chin. Phys. B, 2024, 33 (**6**): 060202. DOI: 10.1088/1674-1056/ad24d5

Bifurcation and dynamics in double-delayed Chua circuits with periodic perturbation

Wenjie Yang(杨文杰)
Chin. Phys. B, 2022, 31 (**2**): 020201. DOI: 10.1088/1674-1056/ac1e0b

Finite-time Mittag-Leffler synchronization of fractional-order delayed memristive neural networks with parameters uncertainty and discontinuous activation functions

Chong Chen(陈冲), Zhixia Ding(丁芝侠), Sai Li(李赛), Liheng Wang(王利恒)
Chin. Phys. B, 2020, 29 (**4**): 040202. DOI: 10.1088/1674-1056/ab7803

Stability switching and hopf bifurcation in a two-delay predation system with diffusion and network coupling

Wenjie Yang(杨文杰)[1,2,3], Jingxin Hu(胡静欣)[1,4], Qianqian Zheng(郑前前)[1], Jianwei Shen(申建伟)[4,†], and Yiping Lin(林怡平)[5]

[1] *School of Science, Xuchang University, Xuchang* 461000, *China*
[2] *Complex Systems Research Center, Shanxi University, Taiyuan* 030006, *China*
[3] *Shanxi Key Laboratory of Mathematical Techniques and Big Data Analysis for Disease Control and Prevention, Taiyuan* 030006, *China*
[4] *School of Mathematics and Statistics, North China University of Water Resources and Electric Power, Zhengzhou* 450046, *China*
[5] *Department of Applied Mathematics, Kunming University of Science and Technology, Kunming* 650500, *China*

(Received 18 January 2026; revised manuscript received 2 April 2026; accepted manuscript online 8 April 2026)

This paper studies stability switching and Hopf bifurcation in a two-delay predation system with diffusion and network coupling. By using the Kronecker-product formulation and Laplacian-mode decomposition, the high-dimensional characteristic equation of the coupled system is reduced to a family of mode-dependent characteristic equations. Based on this reduction, explicit stability-switching curves are derived in the (τ_1, τ_2)-plane, and the corresponding stability region of the positive equilibrium is determined. Furthermore, by applying the Hassard method and center-manifold reduction, the direction of the Hopf bifurcation, the stability of the bifurcating periodic solutions, and the variation of their periods are obtained. Numerical examples are presented to verify the theoretical results and illustrate the temporal and spatiotemporal dynamics generated by the two delays under network coupling. These results provide an effective analytical framework for studying delay-induced stability switching and oscillatory behavior in networked predator-prey systems.

Keywords: predation system, network coupling, stability switching, time delays, Hopf bifurcation

PACS: 02.30.–f, 02.30.Ks, 02.30.Oz, 02.30.Sa

DOI: 10.1088/1674-1056/ae5c8a **CSTR:** 32038.14.CPB.ae5c8a

1. Introduction

In ecology, predation models are classical frameworks for describing species interactions and have long been used to study local population dynamics. Predation systems have been extensively studied in recent years.[1,2] Since the original models were established,[3,4] mathematicians and biologists have progressively refined their descriptions of dynamical behaviors in predation systems. Under standard simplifying assumptions, a commonly used predator-prey model is given by the following system[5]

$$\begin{cases} \dot{x} = rx - kx^2 - \dfrac{mxy}{a+x}, \\ \dot{y} = \dfrac{cmxy}{a+x} - py. \end{cases} \tag{1}$$

However, spatial migration and time-delay effects are ubiquitous in real ecosystems, ranging from population diffusion caused by habitat fragmentation to response delays induced by predator breeding cycles. These factors collectively shape the complex dynamics of ecosystems. In recent years, with the interdisciplinary integration of network science and dynamical systems theory, predation models on undirected networks have attracted increasing attention.[6–9] Such models combine local node dynamics with edge-based coupling, thereby providing a more realistic framework for analyzing ecological processes in discrete spaces.

Diffusion, as the migration process of species in space, quantifies their movement rate through diffusion coefficients. It not only reflects species' responses to resource distribution and environmental pressure but also reshapes population spatial distribution through material exchange between nodes. For example, Miao and Zhu[10] found that in a two-dimensional reaction-diffusion model, the coupling of time delay and diffusion can induce Turing instability, leading to the emergence of spatial patterns such as stripes and spots. This pattern-formation mechanism is particularly important in fragmented habitats. When diffusion interacts with predation and reproduction, species may avoid local extinction through spatially heterogeneous distributions.[11,12]

Time delay originates from inherent delays in ecological processes, such as prey maturation cycles, predator gestation delays, or response intervals to environmental changes. Suriguga *et al.*[13] showed that time delay can lead to bifurcation in a predation model, triggering periodic oscillations in population sizes; Wang *et al.*[14] further discovered that the superposition of prey spatial memory and a delay in predator gestation can exert a regulatory effect on the stability of the positive equilibrium state of the system, even triggering persis-

†Corresponding author. E-mail: xcjwshen@gmail.com

© 2026 Chinese Physical Society and IOP Publishing Ltd. All rights, including for text and data mining, AI training, and similar technologies, are reserved.

tent oscillations under diffusion-free conditions. The dynamical complexity induced by such time delays makes ecosystems exhibit nonlinear responses to parameter changes, increasing the difficulty of predicting population dynamics.[15,16]

Undirected networks, characterized by symmetric connections, provide a natural framework for describing mutualistic or competitive interactions among species. In predation systems, undirected edges usually denote the bidirectional migration of species between adjacent habitats, and topological features such as node degree and clustering coefficient directly influence the diffusion efficiency and stability of the system. For example, Gou *et al.*[17] pointed out that the eigenvalue distribution of the undirected network Laplacian determines the critical bifurcation parameters: fully connected graphs suppress spatial heterogeneous oscillations due to strong coupling effects, while sparse networks may promote non-uniform population distributions.

Embedding diffusion and time delays into undirected network models enables the construction of more realistic ecological scenarios. Taking the Leslie-Gower predation system as an example, when considering time-delay reaction-diffusion under uniform Neumann boundary conditions, Jiao *et al.*[18] found that the system can exhibit spatial Hopf bifurcation, with oscillation patterns closely related to network connection density. Zhou *et al.*[19] further introduced nonlocal intraspecific competition and spatial memory, confirming that memory-based diffusion coefficients significantly alter the system's bifurcation thresholds and oscillation periods. In addition, related studies published in domestic journals have also shown that bifurcation-oriented analysis is important for understanding complex oscillatory behaviors in nonlinear dynamical systems.[20] These studies indicate that the topological structure of undirected networks synergizes with diffusion-delay effects to jointly regulate ecological system dynamics.

Despite substantial progress in the study of predation systems on undirected networks, their high dimensionality and nonlinearity still pose significant theoretical challenges. In existing research, linear stability analyses, such as Turing instability analysis and Hopf bifurcation analysis, have been well developed, but the characterization of complex dynamics after bifurcation (such as the stability of periodic solutions and multi-frequency oscillation mechanisms) still relies on normal form theories. Gou *et al.*[17,21] first proposed a Hopf normal form derivation framework for undirected network reaction-diffusion systems, successfully extending the center manifold reduction method to discrete space models by decomposing the eigenstructure of high-dimensional Jacobian matrices using Kronecker products. However, this framework mainly targets delay-free systems. When introducing multiple time-delays (such as predator response delays and prey migration delays), the analytical calculation of normal form coefficients and the determination of bifurcation curves still face technical bottlenecks. This difficulty involves not only eigenvalue tracking in multi-parameter spaces but also the treatment of delay-induced nonlocal nonlinear couplings.[22]

Additionally, the interaction of multiple ecological factors has motivated the development of more complex systems. For instance, Anand *et al.*[23] incorporated prey fear effects and predator group hunting behavior into undirected network models, revealing that time-delay anti-predation responses can enhance system oscillation amplitudes; Hou and Ding[24] constructed a vector-borne disease-predation system with nonlocal effects and memory diffusion for pine wilt disease transmission, uncovering the regulatory mechanism of network topology on disease transmission thresholds. These studies indicate that the development of undirected network predation systems should focus more on the integration of multi-factor coupling and advanced mathematical methods.[25,26]

This paper studies a two-delay predation system with diffusion and undirected network coupling. The delay τ_1 characterizes the delayed growth effect of the prey, while τ_2 represents the delayed predation effect. Accordingly, we consider the following two-delay predation system:

$$\begin{cases} \dot{x} = rx(t-\tau_1) - kx^2 - \dfrac{mxy(t-\tau_2)}{a+x}, \\ \dot{y} = \dfrac{cmxy}{a+x} - py, \end{cases} \tag{2}$$

where $x(t)$ and $y(t)$ denote the prey and predator densities at time t, respectively. The parameter $r>0$ is the intrinsic growth rate of the prey, and $k=\frac{r}{K}>0$ is the intraspecific competition coefficient, where K is the carrying capacity of the prey. The term $-kx^2$ describes density-dependent self-limitation, and $\frac{mx}{a+x}$ is the Holling type-II functional response. Moreover, $m>0$ denotes the capture rate, $a>0$ is the half-saturation constant, $c>0$ is the conversion efficiency, and $p>0$ is the predator mortality rate.

The main purpose of this paper is to analyze how the two delays affect the local stability and Hopf bifurcation of the positive equilibrium in the networked predation system. By exploiting the Kronecker-product structure and Laplacian-mode decomposition, we reduce the high-dimensional characteristic equation to a family of mode-dependent characteristic equations. This allows us to derive explicit stability-switching curves in the (τ_1,τ_2)-plane and characterize the corresponding Hopf bifurcation properties by means of the Hassard method and center-manifold reduction.

The rest of this paper is organized as follows. Section 2 is devoted to the stability-switching curves of the two-delay predation system with diffusion and network coupling. Section 3 studies the stability and Hopf bifurcation of the system. Section 4 presents numerical simulations to verify the theoretical results and illustrate the corresponding dynamical behaviors.

2. Stability-switching curves of a two-delay predation system with diffusion and network coupling

The basic predation system (2) has the following equilibrium points:

$$E_1=(0,0),\ \ E_2=(\frac{r}{k},0),$$
$$E^*(x^*,y^*)=\left(\frac{pa}{cm-p},\ \frac{-ac(pak-cmr+rp)}{(cm-p)^2}\right).$$

The equilibrium E^* is positive if and only if the conditions $p<cm$ and $(ak+r)p<cmr$ are satisfied.

To incorporate spatial diffusion and network coupling, we introduce the Laplacian matrix and consider the following coupled two-delay predation system:

$$\begin{cases}\dfrac{\mathrm{d}x_i}{\mathrm{d}t}=rx_i(t-\tau_1)-kx_i^2-\dfrac{mx_iy_i(t-\tau_2)}{a+x_i}+k_1\sum_{j=1}^{N}L_{ij}x_j,\\ \dfrac{\mathrm{d}y_i}{\mathrm{d}t}=\dfrac{cmx_iy_i}{a+x_i}-py_i+k_2\sum_{j=1}^{N}L_{ij}y_j.\end{cases}\tag{3}$$

For an undirected network, the Laplacian matrix $L=\{L_{ij}\}$ is symmetric and hence has real eigenvalues together with an orthonormal basis of eigenvectors. Let Λ_l be an eigenvalue of L with corresponding eigenvector ψ_l, $l=1,2,\ldots,N$. Here, k_1 and k_2 denote the diffusion coefficients of the prey and predator populations, respectively.[27] Let $u_i(t)=x_i(t)-x^*$ and $v_i(t)=y_i(t)-y^*$ denote the deviations from the equilibrium E^*. Linearizing system (3) around the equilibrium E^*, we obtain

$$\begin{aligned}\begin{pmatrix}\dot{u}_i\\ \dot{v}_i\end{pmatrix}&=A_{10}\begin{pmatrix}u_i\\ v_i\end{pmatrix}+A_{11}\begin{pmatrix}u_{i,\tau_1}\\ v_{i,\tau_1}\end{pmatrix}+A_{12}\begin{pmatrix}u_{i,\tau_2}\\ v_{i,\tau_2}\end{pmatrix}\\&\quad+K\begin{pmatrix}\sum_{j=1}^{N}L_{ij}u_j\\ \sum_{j=1}^{N}L_{ij}v_j\end{pmatrix},\end{aligned}$$

where

$$A_{10}=\begin{pmatrix}a_{11}&0\\ a_{21}&a_{22}\end{pmatrix},\quad A_{11}=\begin{pmatrix}b_{11}&0\\ 0&0\end{pmatrix},$$
$$A_{12}=\begin{pmatrix}0&c_{12}\\ 0&0\end{pmatrix},\ \ K=\begin{pmatrix}k_1&0\\ 0&k_2\end{pmatrix}.$$

In the above matrices, the coefficients are given by

$$a_{11}=-2kx^*-\frac{amy^*}{(a+x^*)^2},\ \ a_{21}=\frac{cmay^*}{(a+x^*)^2},$$
$$a_{22}=\frac{cmx^*}{a+x^*}-p,\ \ b_{11}=r,\ \ c_{12}=-\frac{mx^*}{a+x^*}.$$

Let $U:=(u_1(t),v_1(t),\ldots,u_N(t),v_N(t))^{\mathrm{T}}$, $U_{\tau_1}:=(u_1(t-\tau_1),v_1(t-\tau_1),\ldots,u_N(t-\tau_1),v_N(t-\tau_1))^{\mathrm{T}}$, $U_{\tau_2}:=(u_1(t-\tau_2),v_1(t-\tau_2),\ldots,u_N(t-\tau_2),v_N(t-\tau_2))^{\mathrm{T}}$. Then above linearizing system can be written in matrix form as

$$\begin{aligned}\frac{\mathrm{d}U}{\mathrm{d}t}&=(I_N\otimes A_{10})U+(I_N\otimes A_{11})U_{\tau_1}\\&\quad+(I_N\otimes A_{12})U_{\tau_2}+(L\otimes K)U,\end{aligned}\tag{4}$$

where I_N is the $N\times N$ identity matrix and $\otimes$ denotes the Kronecker product.

Assume that $\psi_l=(\psi_l^1,\psi_l^2,\ldots,\psi_l^N)^{\mathrm{T}}$ is an eigenvector of the Laplacian matrix L corresponding to the eigenvalue Λ_l, i.e., $L\psi_l=\Lambda_l\psi_l$. Specifically, for $i,l=1,2,\ldots,N$, $\sum_{j=1}^{N}L_{ij}\psi_l^j=\Lambda_l\psi_l^i$.

Substituting $U(t)=\psi_l\otimes C\mathrm{e}^{\lambda t}$, where $C=(C_1,C_2)^{\mathrm{T}}\neq 0$, into system (4), we obtain the characteristic equation associated with the mode Λ_l

$$\begin{aligned}&\det(\lambda I_{2N}-(I_N\otimes A_{10})-(I_N\otimes A_{11})\mathrm{e}^{-\lambda\tau_1}\\&-(I_N\otimes A_{12})\mathrm{e}^{-\lambda\tau_2}-(L\otimes K))=0.\end{aligned}$$

Accordingly, the stability of the linearized system is determined by the roots of the corresponding characteristic equation. For convenience, we define

$$B:=I_N\otimes A_{10}+I_N\otimes\left(\mathrm{e}^{-\lambda\tau_1}A_{11}\right)+I_N\otimes\left(\mathrm{e}^{-\lambda\tau_2}A_{12}\right)+L\otimes K.$$

We now state the following result.

Theorem 1 For the mode matrices

$$B_l=A_{10}+\mathrm{e}^{-\lambda\tau_1}A_{11}+\mathrm{e}^{-\lambda\tau_2}A_{12}+\Lambda_lK,\ l=1,2,\ldots,N$$

if B_l has eigenvalue λ (with corresponding eigenvector $C_l=(C_{l1},C_{l2})^{\mathrm{T}}$ satisfying $B_lC_l=\lambda C_l$), then λ is also an eigenvalue of B. The corresponding eigenvector of B is $\psi_l\otimes C_l$.

Proof By direct calculation (for each $l=1,2,\ldots,N$),

$$\begin{aligned}B(\psi_l\otimes C_l)&=\Big(I_N\otimes A_{10}+I_N\otimes\left(\mathrm{e}^{-\lambda\tau_1}A_{11}\right)\\&\quad+I_N\otimes\left(\mathrm{e}^{-\lambda\tau_2}A_{12}\right)+L\otimes K\Big)(\psi_l\otimes C_l)\\&=(I_N\otimes A_{10})(\psi_l\otimes C_l)+\left(I_N\otimes\left(\mathrm{e}^{-\lambda\tau_1}A_{11}\right)\right)(\psi_l\otimes C_l)\\&\quad+\left(I_N\otimes\left(\mathrm{e}^{-\lambda\tau_2}A_{12}\right)\right)(\psi_l\otimes C_l)+(L\otimes K)(\psi_l\otimes C_l)\\&=(I_N\psi_l)\otimes(A_{10}C_l)+(I_N\psi_l)\otimes\left(\mathrm{e}^{-\lambda\tau_1}A_{11}C_l\right)\\&\quad+(I_N\psi_l)\otimes\left(\mathrm{e}^{-\lambda\tau_2}A_{12}C_l\right)+(L\psi_l)\otimes(KC_l)\\&=\psi_l\otimes(A_{10}C_l)+\psi_l\otimes\left(\mathrm{e}^{-\lambda\tau_1}A_{11}C_l\right)\\&\quad+\psi_l\otimes\left(\mathrm{e}^{-\lambda\tau_2}A_{12}C_l\right)+\Lambda_l\psi_l\otimes(KC_l)\\&=\psi_l\otimes(A_{10}C_l+\mathrm{e}^{-\lambda\tau_1}A_{11}C_l+\mathrm{e}^{-\lambda\tau_2}A_{12}C_l+\Lambda_lKC_l)\\&=\psi_l\otimes(B_lC_l)\\&=\psi_l\otimes(\lambda C_l)\\&=\lambda(\psi_l\otimes C_l).\end{aligned}$$

Thus, $B(\psi_l\otimes C_l)=\lambda(\psi_l\otimes C_l)$.

Then, expanding $\det(B_l - \lambda I_2) = 0$, we obtain the characteristic equation for each mode l

$$\lambda^2 + \alpha_{l1}\lambda + \alpha_{l2} + \mathrm{e}^{-\lambda\tau_1}(\alpha_{l3}\lambda + \alpha_{l4}) + \mathrm{e}^{-\lambda\tau_2}\alpha_{l5} = 0, \quad (5)$$

where $\alpha_{l1} = -(k_1\Lambda_l + k_2\Lambda_l + a_{11} + a_{22})$, $\alpha_{l2} = a_{11}a_{22} + (a_{11}k_2 + a_{22}k_1)\Lambda_l + k_1k_2\Lambda_l^2$, $\alpha_{l3} = -b_{11}$, $\alpha_{l4} = b_{11}k_2\Lambda_l + a_{22}b_{11}$, $\alpha_{l5} = -c_{12}a_{21}$.

Since our interest lies in the coexistence state, we focus on the positive equilibrium E^*. We next analyze system (3) in the following two cases.

Case 1 Delay-free ($\tau_1 = \tau_2 = 0$).

When $\tau_1 = \tau_2 = 0$, Eq. (5) reduces to

$$\lambda^2 + (\alpha_{l1} + \alpha_{l3})\lambda + \alpha_{l2} + \alpha_{l4} + \alpha_{l5} = 0. \quad (6)$$

By the Routh-Hurwitz criterion, the positive equilibrium E^* is locally asymptotically stable if and only if $\alpha_{l1} + \alpha_{l3} > 0$ and $(\alpha_{l1} + \alpha_{l3})(\alpha_{l2} + \alpha_{l4} + \alpha_{l5}) > 0$ for all $l = 1, 2, \ldots, N$. This condition gives the local stability criterion for the positive equilibrium in the delay-free case.

Case 2 Delay-included (τ_1 and τ_2 are not both zero).

We rewrite Eq. (5) in the form

$$P_l(\lambda, \tau_1, \tau_2) = P_{l0}(\lambda) + P_{l1}(\lambda)\mathrm{e}^{-\lambda\tau_1} + P_{l2}(\lambda)\mathrm{e}^{-\lambda\tau_2} = 0, \quad (7)$$

where $P_{l0}(\lambda) = \lambda^2 + \alpha_{l1}\lambda + \alpha_{l2}$, $P_{l1}(\lambda) = \alpha_{l3}\lambda + \alpha_{l4}$, $P_{l2}(\lambda) = \alpha_{l5}$. The following result is based on Ref. [28].

From the above conditions, we obtain the following lemma.

Lemma 1 For each $\omega > 0$, the following statements hold.

(1) If $P_{l0}(\mathrm{i}\omega) \neq 0$ and $(\tau_1, \tau_2) \in R_+^2$, then $\lambda = \mathrm{i}\omega$ can be a solution of $P_l(\lambda, \tau_1, \tau_2) = 0$ if and only if

$$|P_{l1}(\mathrm{i}\omega)| + |P_{l2}(\mathrm{i}\omega)| \geq |P_{l0}(\mathrm{i}\omega)|, \quad (8)$$

$$-|P_{l0}(\mathrm{i}\omega)| \leq |P_{l1}(\mathrm{i}\omega)| - |P_{l2}(\mathrm{i}\omega)| \leq |P_{l0}(\mathrm{i}\omega)|. \quad (9)$$

(2) If $P_{l0}(\mathrm{i}\omega) = 0$ and $(\tau_1, \tau_2) \in R_+^2$, then $\lambda = \mathrm{i}\omega$ can be a solution of $P_l(\lambda, \tau_1, \tau_2) = 0$ if and only if

$$|P_{l1}(\mathrm{i}\omega)| = |P_{l2}(\mathrm{i}\omega)|.$$

For convenience, conditions (8) and (9) can be rewritten as

$$\begin{aligned} F_{l1} &= |P_{l1}(\mathrm{i}\omega)| - |P_{l2}(\mathrm{i}\omega)| - |P_{l0}(\mathrm{i}\omega)|, \\ F_{l2} &= |P_{l2}(\mathrm{i}\omega)| - |P_{l1}(\mathrm{i}\omega)| - |P_{l0}(\mathrm{i}\omega)|, \\ F_{l3} &= |P_{l0}(\mathrm{i}\omega)| - |P_{l1}(\mathrm{i}\omega)| - |P_{l2}(\mathrm{i}\omega)|. \end{aligned} \quad (10)$$

Therefore, $\lambda = \mathrm{i}\omega$ is a solution of $P_l(\lambda, \tau_1, \tau_2) = 0$ if and only if the inequalities $F_{l1} \leq 0, F_{l2} \leq 0, F_{l3} \leq 0$ hold. We denote by Ω_l the set of all positive ω satisfying Eqs. (8) and (9). For any given $\omega_0 \in \Omega_l$ with $P_{lk}(\mathrm{i}\omega) \neq 0$ for $k = 0, 1, 2$, it follows from Eq. (10) that the pair (τ_1, τ_2) satisfies

$$\begin{aligned} &\tau_{l10} = \tau_{l1}^{\mu\pm}(\omega_0) = \frac{\arg\frac{P_{l1}(\mathrm{i}\omega)}{P_{l0}(\omega)} + (2\mu - 1)\pi \pm \theta_{l1}}{\omega_0} \geq 0, \\ &\mu = \mu_0^{\pm},\ \mu_0^{\pm} + 1, \ldots, \end{aligned} \quad (11)$$

$$\begin{aligned} &\tau_{l20} = \tau_{l2}^{\nu\pm}(\omega_0) = \frac{\arg\frac{P_{l2}(\mathrm{i}\omega)}{P_{l0}(\omega)} + (2\nu - 1)\pi \mp \theta_{l2}}{\omega_0} \geq 0, \\ &\nu = \nu_0^{\pm},\ \nu_0^{\pm} + 1, \ldots, \end{aligned} \quad (12)$$

where $\theta_{l1}, \theta_{l2} \in [0, \pi]$ are

$$\begin{aligned} \theta_{l1} &= \cos^{-1}\left(\frac{|P_{l0}(\mathrm{i}\omega_0)|^2 + |P_{l1}(\mathrm{i}\omega_0)|^2 - |P_{l2}(\mathrm{i}\omega_0)|^2}{2|P_{l0}(\mathrm{i}\omega_0)||P_{l1}(\mathrm{i}\omega_0)|}\right), \\ \theta_{l2} &= \cos^{-1}\left(\frac{|P_{l0}(\mathrm{i}\omega_0)|^2 + |P_{l2}(\mathrm{i}\omega_0)|^2 - |P_{l1}(\mathrm{i}\omega_0)|^2}{2|P_{l0}(\mathrm{i}\omega_0)||P_{l2}(\mathrm{i}\omega_0)|}\right), \end{aligned}$$

and μ_0^+, μ_0^-, ν_0^+, ν_0^- represent the smallest feasible integers (which might be negative and potentially depend on ω_0) such that the corresponding $\tau_{l1}^{\mu_0^+ +}$, $\tau_{l1}^{\mu_0^- -}$, $\tau_{l2}^{\nu_0^+ +}$, $\tau_{l2}^{\nu_0^- -}$ values computed are non-negative. Hence, for each $\omega_0 \in \Omega_l$, formulas (11) and (12) determine the corresponding stability-switching curves in the τ_1–τ_2 plane. Differentiating the characteristic Eq. (7) with respect to τ_1 and τ_2, we obtain the transversal conditions

$$\begin{aligned} \mathrm{Re}\left[\frac{\mathrm{d}\lambda}{\mathrm{d}\tau_1}\right]^{-1}_{\tau_1=\tau_{l10}} &= \frac{2\alpha_{l3}\sin(\omega_0\tau_{l10})\omega_0^2 + M_{l11}\omega_0 + M_{l12}}{\alpha_{l3}^2\omega_0^3 + \alpha_{l4}\omega_0^6}, \\ \mathrm{Re}\left[\frac{\mathrm{d}\lambda}{\mathrm{d}\tau_2}\right]^{-1}_{\tau_2=\tau_{l20}} &= \frac{M_{l21}\omega_0 + M_{l22}}{\alpha_{l5}\omega_0}, \end{aligned}$$

where

$$\begin{aligned} M_{l11} &= [\cos(\omega_0\tau_{l20})\alpha_{l3}\alpha_{l5}\tau_{l20} - \alpha_{l1}\alpha_{l3} + 2\alpha_{l4}]\cos(\omega_0\tau_{l10}) \\ &\quad + \alpha_{l3}(\sin(\omega_0\tau_{l10})\sin(\omega_0\tau_{l20})\alpha_{l3}\tau_{l10} - \alpha_{l3}), \\ M_{l12} &= \alpha_{l4}[\sin(\omega_0\tau_{l10})(\alpha_{l1} - \cos(\omega_0\tau_{l20})\alpha_{l5}\tau_{l20}) \\ &\quad + \cos(\omega_0\tau_{l10})\sin(\omega_0\tau_{l20})\alpha_{l5}\tau_{l20}], \\ M_{l21} &= [-\tau_{l20}\alpha_{l3}\cos(\omega_0\tau_{l10}) + 2]\cos(\omega_0\tau_{l20}) \\ &\quad - \sin(\omega_0\tau_{l20})\tau_{l10}\alpha_{l3}\sin(\omega_0\tau_{l10}), \\ M_{l22} &= (\tau_{l10}\alpha_{l4} - \alpha_{l3})\sin(\omega_0\tau_{l10})\cos(\omega_0\tau_{l20}) \\ &\quad - [(\tau_{l10}\alpha_{l4} - \alpha_{l3})\cos(\omega_0\tau_{l10}) - \alpha_{l1}]\sin(\omega_0\tau_{l20}). \end{aligned}$$

Let

$$2\alpha_{l3}\sin(\omega_0\tau_{l10})\omega_0^2 + M_{l11}\omega_0 + M_{l12} \neq 0, \quad (13)$$

$$M_{l21}\omega_0 + M_{l22} \neq 0. \quad (14)$$

For each mode l, let T_l^j denote the j-th continuous curve segment parameterized by ω_0, and let T_l^0 denote the interior region enclosed by the coordinate axes and these curves.

Moreover, let $T_l = \bigcup_{j=1}^{m} T_l^j$, which constitutes the stability-switching curves.

Based on the above analysis, we obtain the following theorem on the stability switching of the positive equilibrium E^*.

Theorem 2 Assume that conditions (13) and (14) hold. Let $T_l^j = (\tau_{l10}^j(\omega_0), \tau_{l20}^j(\omega_0))$ denote the curve segments on Ω_l, and let T_l^0 denote the corresponding interior region. For E^* of Eq. (3):

(I) If $(\tau_1, \tau_2) \in T_l^0$, then E^* is asymptotically stable;

(II) If $(\tau_1, \tau_2) \in T_l^j$, then Eq. (5) has a pair of purely imaginary roots, and a Hopf bifurcation occurs at E^*.

To implement Theorem 2 numerically, we summarize the procedure for computing the stability-switching curves in the (τ_1, τ_2)-plane as follows.

Algorithm 1 Numerical computation of the stability-switching curves.

1: Step 1. Fix a Laplacian eigenvalue Λ_l and compute the functions $F_{l1}(\omega)$, $F_{l2}(\omega)$, and $F_{l3}(\omega)$ for $\omega > 0$.
2: Step 2. Determine the admissible frequency set $\Omega_l = \{\omega > 0 : F_{l1}(\omega) \le 0,\ F_{l2}(\omega) \le 0,\ F_{l3}(\omega) \le 0\}$.
3: Step 3. For each $\omega \in \Omega_l$, compute $\theta_{l1}(\omega)$ and $\theta_{l2}(\omega)$, and then evaluate $\tau_1(\omega)$ and $\tau_2(\omega)$ from Eqs. (11)–(12).
4: Step 4. Choose the smallest integers μ and ν such that $\tau_1(\omega) \ge 0$ and $\tau_2(\omega) \ge 0$.
5: Step 5. Use the signs of $\mathrm{Re}(\mathrm{d}\lambda/\mathrm{d}\tau_1)$ and $\mathrm{Re}(\mathrm{d}\lambda/\mathrm{d}\tau_2)$ to determine the crossing direction.
6: Step 6. Plot the curves in the (τ_1, τ_2)-plane and identify the stable region according to Theorem 2.

3. The stability associated with the Hopf bifurcation

By employing the Hassard method and center manifold theorem,[29] we investigate the stability of the Hopf bifurcation and derive the conditions for the bifurcation direction and the stability of bifurcating periodic solutions at the critical value (τ_{l10}, τ_{l20}). We consider two scenarios: $0 < \tau_{l20} \le \tau_{l10}$ and $0 < \tau_{l10} < \tau_{l20}$.

(I) $0 < \tau_{l20} \le \tau_{l10}$

Let $\tau_1 = \tau_{l10} + \mu$, $\mu \in R$, $t = t\tau_1$, $x_l(t\tau_1) = \hat{x}_l(t)$, $y_l(t\tau_1) = \hat{y}_l(t)$. Note that $x_l = \hat{x}_l$ and $y_l = \hat{y}_l$, and denote the solution of Eq. (3) by $x(t) = (x_1(t), y_1(t), \ldots, x_N(t), y_N(t))^{\mathrm{T}}$. Set $x_t(\theta) = x(t+\theta)$, $\theta \in [-1, 0]$, and $x_t \in C([-1,0], R^{2N}) \doteq C_1$. It can be ascertained that at the critical value $\tau_1 = \tau_{l10}$, Eq. (3) experiences a Hopf bifurcation, with the corresponding eigenvalues being $\pm \mathrm{i}\omega_0$. Thereafter, we represent Eq. (3) in the vicinity of E^* as follows:

$$\dot{x}_t = L_\mu(x_t) + g_\mu(x_t), \tag{15}$$

where $L_\mu, g_\mu : C_1 \to R^{2N}$ are linear and nonlinear operators, respectively. The linear operator L_μ is defined as

$$\begin{aligned} L_\mu \upsilon \ =\ & (\tau_{l10}+\mu)\Bigg[(I_N \otimes A_{10}) \operatorname{col}\begin{pmatrix} \upsilon_{l1}(0) \\ \upsilon_{l2}(0) \end{pmatrix}_{l=1}^{N} \\ & + (I_N \otimes A_{11}) \operatorname{col}\begin{pmatrix} \upsilon_{l1}(-\frac{\tau_{l20}}{\tau_1}) \\ \upsilon_{l2}(-\frac{\tau_{l20}}{\tau_1}) \end{pmatrix}_{l=1}^{N} \\ & + (I_N \otimes A_{12}) \operatorname{col}\begin{pmatrix} \upsilon_{l1}(-1) \\ \upsilon_{l2}(-1) \end{pmatrix}_{l=1}^{N} \\ & + (L \otimes K) \operatorname{col}\begin{pmatrix} \upsilon_{l1}(0) \\ \upsilon_{l2}(0) \end{pmatrix}_{l=1}^{N} \Bigg], \end{aligned}$$

and the nonlinear operator g_μ is given by

$$g_\mu(\psi) = (\tau_{l10}+\mu) \operatorname{col}\begin{pmatrix} K_{l1} \\ K_{l2} \end{pmatrix}_{l=1}^{N},$$

where $A_{10}, A_{11}, A_{12}, L, K$ are defined in Eq. (4)

$$\begin{aligned} K_{l1} =\ & \frac{may^*\upsilon_{l1}^2(0)}{(a+x^*)^3} - k\upsilon_{l1}^2(0) - \frac{ma\upsilon_{l1}(0)\upsilon_{l2}(-\frac{\tau_{l20}}{\tau_1})}{(a+x^*)^2} \\ & - \frac{may^*\upsilon_{l1}^3(0)}{(a+x^*)^4} + \frac{ma\upsilon_{l1}^2(0)\upsilon_{l2}(-\frac{\tau_{l20}}{\tau_1})}{(a+x^*)^3} + \text{h.o.t.}, \\ K_{l2} =\ & \frac{cma\upsilon_{l1}(0)\upsilon_{l2}(0)}{(a+x^*)^2} - \frac{y^*cma\upsilon_{l1}^2(0)}{(a+x^*)^3} \\ & + \frac{y^*cma\upsilon_{l1}^3(0)}{(a+x^*)^4} - \frac{cma\upsilon_{l1}^2(0)\upsilon_{l2}(0)}{(a+x^*)^3} + \text{h.o.t.} \end{aligned}$$

According to the Riesz representation theorem, there exists a bounded variational matrix function $\eta(\theta,\mu)_{2N\times 2N}$ for $\theta \in [-1,0]$, such that $L_\mu \upsilon$ satisfies

$$L_\mu \upsilon = \int_{-1}^{0} \mathrm{d}\eta(\theta,\mu)\upsilon(\theta), \ \text{ for } \ \upsilon \in C_1.$$

In fact, we can take

$$\eta(\theta,\mu) = \begin{cases} (\tau_{l10}+\mu)(I_N\otimes A_{10} + I_N \otimes A_{11} \\ \quad + I_N \otimes A_{12} + L \otimes K), & \theta = 0, \\ (\tau_{l10}+\mu)(I_N \otimes A_{11} + I_N \otimes A_{12}), & \theta \in \left[-\frac{\tau_{l20}}{\tau_{l10}}, 0\right), \\ (\tau_{l10}+\mu) I_N \otimes A_{12}, & \theta \in \left(-1, -\frac{\tau_{l20}}{\tau_{l10}}\right), \\ 0, & \theta = -1. \end{cases}$$

For $\phi \in C_1$, define

$$A(\mu)\phi = \begin{cases} \dfrac{\mathrm{d}\phi(\theta)}{\mathrm{d}\theta}, & \theta \in [-1,0), \\ \int_{-1}^{0} \mathrm{d}\eta(\mu,s)\phi(s), & \theta = 0, \end{cases}$$

$$R(\mu)\phi = \begin{cases} 0, & \theta \in [-1,0), \\ f(\mu,\phi), & \theta = 0. \end{cases}$$

When $\theta = 0$, system (15) is equivalent to the following equation:

$$\dot{x}_t = A(\mu)x_t + R(\mu)x_t, \tag{16}$$

where $x_t(\theta) = x(t+\theta)$, $\theta \in [-1,0]$. Denote $A = A(0)$ and $\eta(\theta) = \eta(\theta, 0)$.

For $\upsilon \in C^1([0,1],(\mathbb{R}^{2N})^*)$, define

$$A^*\upsilon(s)=\begin{cases}-\dfrac{\mathrm{d}\upsilon(s)}{\mathrm{d}s}, & s\in(0,1],\\ \int_{-1}^{0}\mathrm{d}\eta^{\mathrm{T}}(0,t)\upsilon(-t), & s=0,\end{cases}$$

and the bilinear inner product

$$\langle\upsilon(s),\phi(\theta)\rangle=\overline{\upsilon}(0)\phi(0)-\int_{-1}^{0}\int_{\xi=0}^{\theta}\overline{\upsilon}(\xi-\theta)\mathrm{d}\eta(\theta)\phi(\xi)\mathrm{d}\xi.$$

Then A and A^* are adjoint operators. It is known that $\pm\mathrm{i}\omega_0\tau_{l10}$ are eigenvalues of A. Therefore, they are also eigenvalues of A^*.

Suppose that the linear operator A has a pair of purely imaginary eigenvalues $\pm\mathrm{i}\omega_0\tau_{l10}$ corresponding to the eigenvectors $q(\theta)$ and $\bar{q}(\theta)$. Then $Aq(\theta)=\mathrm{i}\omega_0\tau_{l10}q(\theta)$. By calculation, we have

$$q(\theta)=\mathrm{e}^{\mathrm{i}\omega_0\tau_{l10}\theta}\cdot\psi_l\otimes\begin{pmatrix}1\\ q_{l1}\end{pmatrix}=\mathrm{e}^{\mathrm{i}\omega_0\tau_{l10}\theta}\cdot\mathrm{col}\begin{pmatrix}\psi_l^j\\ q_{l1}\psi_l^j\end{pmatrix}_{j=1}^{j=N},$$

where

$$q_{l1}=\frac{\mathrm{i}\omega_0-(a_{22}+k_2\Lambda_l)}{a_{21}}.$$

Similarly, we can obtain $q^*(s)$ as an eigenvector of A^* corresponding to the eigenvalue $-\mathrm{i}\omega_0\tau_{l10}$, where

$$\begin{aligned}q^*(s)&=\overline{D}\mathrm{e}^{\mathrm{i}\omega_0\tau_{l10}s}\cdot\psi_l^*\otimes\begin{pmatrix}1\\ q_{l1}^*\end{pmatrix}\\&=\overline{D}\mathrm{e}^{\mathrm{i}\omega_0\tau_{l10}s}\cdot\mathrm{col}\begin{pmatrix}\psi_l^{j*}\\ q_{l1}^*\psi_l^{j*}\end{pmatrix}_{j=1}^{j=N},\end{aligned}$$

where the component is given by

$$q_{l1}^*=\frac{c_{12}\mathrm{e}^{-\mathrm{i}\omega_0\tau_{l20}}}{\mathrm{i}\omega_0-(a_{22}+k_2\Lambda_l)}.$$

ψ_l is the real eigenvector of the network Laplacian matrix L with corresponding eigenvalue Λ_l, and ψ_l^* is the real eigenvector of the matrix L^{T} corresponding to the eigenvalue Λ_l. Now, we calculate the inner product $\langle q^*(s),q(\theta)\rangle$ as follows:

$$\begin{aligned}\langle q^*(s),q(\theta)\rangle&=\overline{D}(\overline{\psi_l^*}\otimes(1,\overline{q_{l1}^*}))(\psi_l\otimes(1,q_{l1}))^{\mathrm{T}}\\&\quad-\int_{-1}^{0}\int_{\xi=\theta}^{0}\overline{D}(\overline{\psi_l^*}\otimes(1,\overline{q_{l1}^*}))\mathrm{e}^{-\mathrm{i}(\xi-\theta)\omega_0\tau_{l10}}\\&\quad\times\mathrm{d}\eta(\theta)(\psi_l\otimes(1,q_{l1}))^{\mathrm{T}}\mathrm{e}^{\mathrm{i}\xi\omega_0\tau_{l10}}\mathrm{d}\xi\\&=\overline{D}(\sum_{j=1}^{N}\psi_l^j\overline{\psi_l^{j*}}(1+q_{l1}\overline{q_{l1}^*}\\&\quad-\int_{-1}^{0}(\overline{\psi_l^*}\otimes(1,\overline{q_{l1}^*}))\mathrm{e}^{\mathrm{i}\theta\omega_0\tau_{l10}}\\&\quad\times\mathrm{d}\eta(\theta)(\psi_l\otimes(1,q_{l1}))^{\mathrm{T}}))\\&=\overline{D}\sum_{j=1}^{N}\psi_l^j\overline{\psi_l^{j*}}(1+q_{l1}\overline{q_{l1}^*}\\&\quad+\tau_{l10}b_{11}\mathrm{e}^{-\mathrm{i}\omega_0\tau_{l10}}+q_{l1}\tau_{l20}c_{12}\mathrm{e}^{-\mathrm{i}\omega_0\tau_{l20}}).\end{aligned}$$

Then we note $\overline{D}=[\sum_{j=1}^{N}\psi_l^j\overline{\psi_l^{j*}}(1+q_{l1}\overline{q_{l1}^*}+\tau_{l10}b_{11}\mathrm{e}^{-\mathrm{i}\omega_0\tau_{l10}}+q_{l1}\tau_{l20}c_{12}\mathrm{e}^{-\mathrm{i}\omega_0\tau_{l20}})]^{-1}$, where the normalization conditions $\langle q^*(t),q(\theta)\rangle=1$ and $\langle q^*(t),\bar{q}(\theta)\rangle=0$ are satisfied.

Let x_t be the solution of Eq. (16) when $\mu=\mu_0$. Then we decompose $\mathbb{R}^{2N}=T^{\mathrm{c}}\oplus T^{\mathrm{su}}$, where $T^{\mathrm{c}}:=\{zq(\theta)+\overline{z\bar{q}}(\theta)|z\in\mathbb{C}\}$ and $T^{\mathrm{su}}:=\{x_t|\langle q^*,x_t\rangle=0\}$. For any

$$x_t(\theta)=(x_{1t}(\theta),y_{1t}(\theta),\cdots,x_{Nt}(\theta),y_{Nt}(\theta))^{\mathrm{T}},$$

there exist $z\in\mathbb{C}$ and

$$W(t,\theta)=\left(W_1^{(1)},W_1^{(2)},\cdots,W_N^{(1)},W_N^{(2)}\right)^{\mathrm{T}}\in T^{\mathrm{su}},$$

such that

$$z(t)=\langle q^*,x_t\rangle,\quad x_t(\theta)=zq(\theta)+\overline{z\bar{q}}(\theta)+W(t,\theta),\quad(17)$$

or, equivalently, in component form

$$\begin{cases}x_l(t)(0)=z\psi_l^j+\bar{z}\overline{\psi_l^j}+W_{j20}^{(1)}(0)\frac{z^2}{2}+W_{j11}^{(1)}(0)z\bar{z}+W_{j02}^{(1)}(0)\frac{\bar{z}^2}{2}\\ \qquad+W_{j30}^{(1)}(0)\frac{z^3}{6}+W_{j21}^{(1)}(0)\frac{z^2\bar{z}}{2}+\cdots,\\ y_l(t)(0)=zq_{l2}\psi_l^j+\overline{zq_{l2}}\overline{\psi_l^j}+W_{j20}^{(2)}(0)\frac{z^2}{2}+W_{j11}^{(2)}(0)z\bar{z}\\ \qquad+W_{j02}^{(2)}(0)\frac{\bar{z}^2}{2}+W_{j30}^{(2)}(0)\frac{z^3}{6}+W_{j21}^{(2)}(0)\frac{z^2\bar{z}}{2}+\cdots,\\ x_l(t)(-1)=z\psi_l^j\mathrm{e}^{-\mathrm{i}\omega_0\tau_{l10}}+\bar{z}\overline{\psi_l^j}\mathrm{e}^{\mathrm{i}\omega_0\tau_{l10}}+W_{j20}^{(1)}(-1)\frac{z^2}{2}\\ \qquad+W_{j11}^{(1)}(-1)z\bar{z}+W_{j02}^{(1)}(-1)\frac{\bar{z}^2}{2}+W_{j30}^{(1)}(-1)\frac{z^3}{6}\\ \qquad+W_{j21}^{(1)}(-1)\frac{z^2\bar{z}}{2}+\cdots,\\ y_l(t)(-1)=zq_{l2}\psi_l^j\mathrm{e}^{-\mathrm{i}\omega_0\tau_{l10}}+\overline{zq_{l2}}\overline{\psi_l^j}\mathrm{e}^{\mathrm{i}\omega_0\tau_{l10}}+W_{j20}^{(2)}(-1)\frac{z^2}{2}\\ \qquad+W_{j11}^{(2)}(-1)z\bar{z}+W_{j02}^{(2)}(-1)\frac{\bar{z}^2}{2}\\ \qquad+W_{j30}^{(2)}(-1)\frac{z^3}{6}+W_{j21}^{(2)}(-1)\frac{z^2\bar{z}}{2}+\cdots,\\ x_l(t)\left(-\frac{\tau_2}{\tau_{l10}}\right)=z\psi_l^j\mathrm{e}^{-\mathrm{i}\omega_0\tau_2}+\bar{z}\overline{\psi_l^j}\mathrm{e}^{\mathrm{i}\omega_0\tau_2}+W_{j20}^{(1)}\left(-\frac{\tau_2}{\tau_{l10}}\right)\frac{z^2}{2}\\ \qquad+W_{j11}^{(1)}\left(-\frac{\tau_2}{\tau_{l10}}\right)z\bar{z}+W_{j02}^{(1)}\left(-\frac{\tau_2}{\tau_{l10}}\right)\frac{\bar{z}^2}{2}\\ \qquad+W_{j30}^{(1)}\left(-\frac{\tau_2}{\tau_{l10}}\right)\frac{z^3}{6}+W_{j21}^{(1)}\left(-\frac{\tau_2}{\tau_{l10}}\right)\frac{z^2\bar{z}}{2}+\cdots,\\ y_l(t)\left(-\frac{\tau_2}{\tau_{l10}}\right)=zq_{l2}\psi_l^j\mathrm{e}^{-\mathrm{i}\omega_0\tau_2}+\overline{zq_{l2}}\overline{\psi_l^j}\mathrm{e}^{\mathrm{i}\omega_0\tau_2}\\ \qquad+W_{j20}^{(2)}\left(-\frac{\tau_2}{\tau_{l10}}\right)\frac{z^2}{2}+W_{j11}^{(2)}\left(-\frac{\tau_2}{\tau_{l10}}\right)z\bar{z}\\ \qquad+W_{j02}^{(2)}\left(-\frac{\tau_2}{\tau_{l10}}\right)\frac{\bar{z}^2}{2}+W_{j30}^{(2)}\left(-\frac{\tau_2}{\tau_{l10}}\right)\frac{z^3}{6}\\ \qquad+W_{j21}^{(2)}\left(-\frac{\tau_2}{\tau_{l10}}\right)\frac{z^2\bar{z}}{2}+\cdots,\end{cases}$$

for $j,l=1,2,\ldots,N$. On the center manifold C_{μ_0}, we have

$$W(t,\theta)=W(z(t),\bar{z}(t),\theta)$$

$$= W_{20}(\theta)\frac{z^2}{2}+W_{11}(\theta)z\bar{z}+W_{02}(\theta)\frac{\bar{z}^2}{2} +W_{30}(\theta)\frac{z^3}{6}+\cdots,$$

where z and $\bar{z}$ represent the local coordinates of the center manifold C_{μ_0} in the directions of q and $\bar{q}$, respectively. Note that if x_t is real, then W is also real. We only consider real solutions. For the solution $x_t \in C_{\mu_0}$ of Eq. (16), since $\mu=\mu_0$, we have

$$\begin{aligned}\dot{z} &= \langle q^*,\dot{x}_t\rangle = \langle q^*,Ax_t+Rx_t\rangle = \langle A^*q^*,x_t\rangle+\langle q^*,Rx_t\rangle\\ &= \mathrm{i}\omega_0\tau_{l10}\langle q^*,x_t\rangle+\langle q^*,Rx_t\rangle\\ &= \mathrm{i}\omega_0\tau_{l10}z+\bar{q}^*(0)f[\mu_0,z(t)q(0)+\bar{z}(t)\bar{q}(0)\\ &\quad +W(z(t),\bar{z}(t),0)]\\ &= \mathrm{i}\omega_0\tau_{l10}z+\bar{q}^*(0)f_0(z,\bar{z}) \triangleq \mathrm{i}\omega_0\tau_{l10}z+g(z,\bar{z}). \end{aligned} \tag{18}$$

Denote

$$\begin{aligned} f_0(z,\bar{z}) &= f_{20}\frac{z^2}{2}+f_{11}z\bar{z}+f_{02}\frac{\bar{z}^2}{2}+f_{21}\frac{z^2\bar{z}}{2}+\cdots,\\ g(z,\bar{z}) &= \bar{q}^*(0)f_0(z,\bar{z}) = g_{20}\frac{z^2}{2}+g_{11}z\bar{z}+g_{02}\frac{\bar{z}^2}{2}\\ &\quad +g_{21}\frac{z^2\bar{z}}{2}+\cdots. \end{aligned}$$

Then

$$\begin{aligned} g_{02} &= \bar{q}^*(0)f_{02}, \quad g_{11} = \bar{q}^*(0)f_{11},\\ g_{20} &= \bar{q}^*(0)f_{20}, \quad g_{21} = \bar{q}^*(0)f_{21}. \end{aligned}$$

To discuss the properties of the periodic solutions of the equation near the origin, it is only necessary to calculate g_{02}, g_{11}, g_{20}, and g_{21}. Below, we give an algorithm for calculating g_{ij}.

Since $f(\mu,\phi)$ is at least quadratic in ϕ, g_{02}, g_{11}, and g_{20} can be directly obtained from Eq. (18), while g_{21} is generally related to the coefficients W_{11} and W_{20} in $W(z,\bar{z},\theta)$. Next, we solve for W_{11} and W_{20}.

From Eqs. (16)–(18), we get

$$\begin{aligned}\dot{W} &= \dot{x}_t-\dot{z}q-\dot{\bar{z}}\bar{q}\\ &= Ax_t+Rx_t-(\mathrm{i}\omega_0\tau_{l10}z+g)q-(-\mathrm{i}\omega_0\tau_{l10}\bar{z}+\bar{g})\bar{q}\\ &= A(W+zq+\bar{z}\bar{q})+Rx_t-2\mathrm{Re}\{gq\}\\ &\quad -\mathrm{i}\omega_0\tau_{l10}zq+\mathrm{i}\omega_0\tau_{l10}\bar{z}\bar{q}\\ &= AW+Rx_t-2\mathrm{Re}\{gq\}. \end{aligned}$$

Thus,

$$\begin{aligned}\dot{W} &= \begin{cases} AW-2\mathrm{Re}\,\overline{q^*}(0)\cdot f_0q(\theta), & -r\le\theta<0,\\ AW-2\mathrm{Re}\,\overline{q^*}(0)\cdot f_0q(\theta)+f_0, & \theta=0, \end{cases}\\ &\triangleq AW+H(z,\bar{z},\theta). \end{aligned} \tag{19}$$

Equation (16) is transformed into

$$\begin{cases}\dot{z}=\mathrm{i}\omega_0\tau_{l10}z+g(z,\bar{z}),\\ \dot{W}=AW+H(z,\bar{z},\theta).\end{cases}$$

Denote

$$\begin{aligned}H(z,\bar{z},\theta) &= H_{20}(\theta)\frac{z^2}{2}+H_{11}(\theta)z\bar{z}\\ &\quad +H_{02}(\theta)\frac{\bar{z}^2}{2}+H_{30}(\theta)\frac{z^3}{6}+\cdots. \end{aligned} \tag{20}$$

On the other hand, in a neighborhood of the origin, we have

$$\dot{W}=W_z\dot{z}+W_{\bar{z}}\dot{\bar{z}}.$$

Therefore, substituting Eqs. (18) and (20) into Eq. (19) and comparing the coefficients of terms with the same degree in z, we obtain

$$(A-I_N\otimes(2\mathrm{i}\omega_0I_2))W_{20}(\theta)=-H_{20}(\theta),\ \ AW_{11}=-H_{11}(\theta). \tag{21}$$

Note that H_{ij} is independent of $W_{ij}(\theta)$ when $i+j=2$. Also, since $2\mathrm{i}\omega_0$ and 0 are not eigenvalues of A, W_{20}, W_{11}, and $W_{02}=\overline{W}_{20}$ can be solved from Eq. (21). That is, from Eq. (21), when $\theta\in[-1,0)$, we have

$$H(z,\bar{z},\theta)=-\bar{q}^*(0)f_0q(\theta)-q^*(0)f_0\bar{q}(\theta)=-gq(\theta)-\overline{gq}(\theta). \tag{22}$$

Comparing the coefficients in Eq. (20), we get

$$H_{20}(\theta)=-g_{20}q(\theta)-\bar{g}_{02}\bar{q}(\theta),\ \ H_{11}(\theta)=-g_{11}q(\theta)-\bar{g}_{11}\bar{q}(\theta).$$

From Eqs. (21) and (22) and the definition of matrix A, we obtain

$$\dot{W}_{20}(\theta)=2\mathrm{i}\omega_0\tau_{l10}W_{20}(\theta)+g_{20}q(\theta)+\bar{g}_{02}\bar{q}(\theta).$$

Note that $q(\theta)=q(0)\mathrm{e}^{\mathrm{i}\omega_0\tau_{l10}\theta}$. Then,

$$\begin{aligned}W_{20}(\theta) &= \frac{\mathrm{i}g_{20}}{\omega_0\tau_{l10}}q(0)\mathrm{e}^{\mathrm{i}\omega_0\tau_{l10}\theta}+\frac{\mathrm{i}\bar{g}_{02}}{3\omega_0\tau_{l10}}\bar{q}(0)\mathrm{e}^{-\mathrm{i}\omega_0\tau_{l10}\theta}\\ &\quad +E_2\mathrm{e}^{2\mathrm{i}\omega_0\tau_{l10}\theta}, \end{aligned} \tag{23}$$

$$\begin{aligned}W_{11}(\theta) &= -\frac{ig_{11}}{\omega_0\tau_{l10}}q(0)\mathrm{e}^{\mathrm{i}\omega_0\tau_{l10}\theta}+\frac{\mathrm{i}\bar{g}_{11}}{\omega_0\tau_{l10}}\bar{q}(0)\mathrm{e}^{-\mathrm{i}\omega_0\tau_{l10}\theta}\\ &\quad +E_1, \end{aligned} \tag{24}$$

where both E_1 and E_2 are $2N$-dimensional constant vectors.

Also, when $\theta=0$, we have

$$\begin{cases}\int_{-r}^{0}\mathrm{d}\eta(\mu_0,\theta)W_{20}(\theta)=2\mathrm{i}\omega_0\tau_{l10}W_{20}(0),\\ \qquad\qquad +g_{02}q(0)+\bar{g}_{02}\bar{q}(0)-f_2,\\ \int_{-r}^{0}\mathrm{d}\eta(\mu_0,\theta)W_{11}(\theta)=g_{11}q(0)+\bar{g}_{11}\bar{q}(0)-f_1.\end{cases} \tag{25}$$

Substitute Eqs. (25) into Eqs (23) and (24) respectively, and note that

$$\begin{cases}(I_N\otimes(\mathrm{i}\omega_0\tau_{l10}I_2)-\int_{-r}^{0}\mathrm{e}^{\mathrm{i}\omega_0\tau_{l10}\theta}\mathrm{d}\eta(\mu_0,\theta))q(0)=0,\\ (-I_N\otimes(\mathrm{i}\omega_0\tau_{l10}I_2)-\int_{-r}^{0}\mathrm{e}^{-\mathrm{i}\omega_0\tau_{l10}\theta}\mathrm{d}\eta(\mu_0,\theta))\bar{q}(0)=0.\end{cases}$$

Then we can calculate that

$$E_2 = 2I_N \otimes \begin{pmatrix} a_{11}+b_{11}\mathrm{e}^{-\mathrm{i}\omega_0\tau_{l10}}+k_1\Lambda_l-2\mathrm{i}\omega_0 & c_{12}\mathrm{e}^{-\mathrm{i}\omega_0\tau_{l20}} \\ a_{21} & a_{22}+k_2\Lambda_l-2\mathrm{i}\omega_0 \end{pmatrix}^{-1} \mathrm{col}\begin{pmatrix} f^j_{l,21} \\ f^j_{l,22} \end{pmatrix}_{j=1}^{j=N},$$

$$E_1 = I_N \otimes \begin{pmatrix} -a_{11}-k_1\Lambda_l-b_{11} & -c_{12} \\ -a_{21} & -a_{22}-k_2\Lambda_l \end{pmatrix}^{-1} \mathrm{col}\begin{pmatrix} f^j_{l,11} \\ f^j_{l,12} \end{pmatrix}_{j=1}^{j=N},$$

where

$$\begin{aligned}
f^j_{l,21} &= \frac{(\psi^j_l)^2}{(a+x^*)^3}[amy^* - amq_{l1}(a+x^*)\mathrm{e}^{-\mathrm{i}\omega_0\tau_{l20}} \\
&\quad -k(a+x^*)^3], \\
f^j_{l,22} &= \frac{amc(\psi^j_l)^2}{(a+x^*)^3}((a+x^*)q_{l1}-y^*), \\
f^j_{l,11} &= \frac{\psi^j_l\overline{\psi^j_l}}{(a+x^*)^3}[2amy^* - 2k(a+x^*)^3 \\
&\quad -am(a+x^*)(q_{l1}\mathrm{e}^{-\mathrm{i}\omega_0\tau_{l20}}+\overline{q_{l1}}\mathrm{e}^{\mathrm{i}\omega_0\tau_{l20}})], \\
f^j_{l,12} &= \frac{amc\psi^j_l\overline{\psi^j_l}}{(a+x^*)^3}((q_{l1}+\overline{q_{l1}})(a+x^*)-2y^*).
\end{aligned}$$

By solving the linear system corresponding to the complement space, we obtain the coefficients g_{ij} as following:

$$\begin{aligned}
g_{20} &= \frac{2\tau_{l10}\overline{D}}{(a+x^*)^3}\sum_{j=1}^{N}(\psi^j_l)^2\overline{\psi^{j*}_l}(amc((a+x^*)q_{l1}-y^*)\overline{q^*_{l1}} \\
&\quad -k(a+x^*)^3+amy^*-amq_{l1}(a+x^*)\mathrm{e}^{-\mathrm{i}\omega_0\tau_{l20}}), \\
g_{11} &= \frac{\tau_{l10}\overline{D}}{(a+x^*)^3}\sum_{j=1}^{N}\psi^j_l\overline{\psi^j_l}\,\overline{\psi^{j*}_l} \\
&\quad \times[amc((q_{l1}+\overline{q_{l1}})(a+x^*)-2y^*)\overline{q^*_{l1}}-2k(a+x^*)^3 \\
&\quad +2amy^*-am(a+x^*)(q_{l1}\mathrm{e}^{-\mathrm{i}\omega_0\tau_{l20}}+\overline{q_{l1}}\mathrm{e}^{\mathrm{i}\omega_0\tau_{l20}})], \\
g_{02} &= \frac{2\tau_{l10}\overline{D}}{(a+x^*)^3}\sum_{j=1}^{N}(\overline{\psi^j_l})^2\overline{\psi^{j*}_l}[amc((a+x^*)\overline{q_{l1}}-y^*)\overline{q^*_{l1}} \\
&\quad -k(a+x^*)^3+amy^*-am\overline{q_{l1}}(a+x^*)\mathrm{e}^{\mathrm{i}\omega_0\tau_{l20}}], \\
g_{21} &= -\frac{\tau_{l10}\overline{D}}{(a+x^*)^4}\sum_{j=1}^{N}\overline{\psi^{j*}_l}[am(a+x^*)^2W^{(2)}_{20}(-\frac{\tau_{l20}}{\tau_{l10}}) \\
&\quad -acm\overline{q^*_{l1}}(a+x^*)^2W^{(2)}_{20}(0)+2am(a+x^*)^2W^{(2)}_{11}(-\frac{\tau_{l20}}{\tau_{l10}}) \\
&\quad -2acm\overline{q^*_{l1}}(a+x^*)^2W^{(2)}_{11}(0)] \\
&\quad +[am\overline{q_{l1}}\,\overline{\psi^j_l}(a+x^*)^2\mathrm{e}^{\mathrm{i}\omega_0\tau_{l20}}+2(a+x^*)(k(a+x^*)^3 \\
&\quad +amy^*(c\overline{q^*_{l1}}-1)-\frac{1}{2}acm\overline{q_{l1}}\,\overline{q^*_{l1}}\,\overline{\psi^j_l}(a+x^*))]W^{(1)}_{20}(0) \\
&\quad +[2amq_{l1}\psi^j_l(a+x^*)^2\mathrm{e}^{-\mathrm{i}\omega_0\tau_{l20}}+4(a+x^*)(k(a+x^*)^3 \\
&\quad +amy^*(c\overline{q^*_{l1}}-1)-\frac{1}{2}acmq_{l1}\psi^j_l\overline{q^*_{l1}}(a+x^*))]W^{(1)}_{11}(0) \\
&\quad -2am(a+x^*)(2q_{l1}\psi^j_l\mathrm{e}^{-\mathrm{i}\omega_0\tau_{l20}}+\overline{q_{l1}}\,\overline{\psi^j_l}\,\mathrm{e}^{\mathrm{i}\omega_0\tau_{l20}}) \\
&\quad +4ma[c\overline{q^*_{l1}}(a+x^*)(q_{l1}\psi^j_l+\frac{1}{2}\overline{q_{l1}}\,\overline{\psi^j_l}) \\
&\quad +\frac{3}{2}y^*(1-c\overline{q^*_{l1}})], \qquad (26)
\end{aligned}$$

and further calculate the key bifurcation parameters.

(i) The direction of the Hopf bifurcation $\mu_2 = -\frac{\mathrm{Re}\{c_1(0)\}}{\mathrm{Re}\{\lambda'(\tau_{l10})\}}$. Precisely, when $\mathrm{Re}\{\lambda'(\tau_{l10})\}>0$, if $\mu_2>0$ (alternatively, $\mu_2<0$), the Hopf bifurcation is supercritical (subcritical, correspondingly), and the periodic solution comes into existence for $\tau_1>\tau_{l10}$ (respectively, $\tau_1<\tau_{l10}$). However, if $\mathrm{Re}\{\lambda'(\tau_{l10})\}<0$, the bifurcating periodic solutions occur in the opposite direction.

(ii) The stability of the bifurcated periodic solutions $\beta_2 = 2\mathrm{Re}(c_1(0))$. More precisely, the bifurcated periodic solutions are stable when $\beta_2<0$; conversely, they are unstable when $\beta_2>0$.

(iii) The period of the bifurcated periodic solutions $T_2 = -\frac{\mathrm{Im}\{c_1(0)\}+\mu_2\mathrm{Im}\{\lambda'(\tau_{l10})\}}{\omega_0\tau_{l10}}$. More precisely, the period increases when $T_2>0$; in contrast, it decreases when $T_2<0$.

Where $c_1(0) = \frac{i}{2\omega_0\tau_{l10}}(g_{20}g_{11}-2|g_{11}|^2-\frac{1}{3}|g_{02}|^2)+\frac{g_{21}}{2}$.

(II) $0<\tau_{l10}<\tau_{l20}$

Let $\tau_2 = \tau_{l20}+\mu_2$. Subsequently, we recast Eq. (3) in the vicinity of E^* as a functional differential equation within the space C_1

$$\dot{x}_t = L_{\mu_2}(x_t)+g_{\mu_2}(x_t),$$

where

$$\begin{aligned}
L_{\mu_2}\upsilon &= (\tau_{l20}+\mu_2)\Bigg[(I_N\otimes A_{10})\,\mathrm{col}\begin{pmatrix}\upsilon_{l1}(0)\\ \upsilon_{l2}(0)\end{pmatrix}_{l=1}^{N} \\
&\quad +(I_N\otimes A_{11})\,\mathrm{col}\begin{pmatrix}\upsilon_{l1}(-1)\\ \upsilon_{l2}(-1)\end{pmatrix}_{l=1}^{N} \\
&\quad +(I_N\otimes A_{12})\,\mathrm{col}\begin{pmatrix}\upsilon_{l1}\left(-\frac{\tau_{l10}}{\tau_2}\right)\\ \upsilon_{l2}\left(-\frac{\tau_{l10}}{\tau_2}\right)\end{pmatrix}_{l=1}^{N} \\
&\quad +(L\otimes K)\,\mathrm{col}\begin{pmatrix}\upsilon_{l1}(0)\\ \upsilon_{l2}(0)\end{pmatrix}_{l=1}^{N}\Bigg],
\end{aligned}$$

$$g_{\mu_2}(\upsilon) = (\tau_{l20}+\mu_2)\,\mathrm{col}\begin{pmatrix}K^*_{l1}\\ K^*_{l2}\end{pmatrix}_{l=1}^{N},$$

$$\begin{aligned}
K^*_{l1} &= \frac{may^*\upsilon^2_{l1}(0)}{(a+x^*)^3}-k\upsilon^2_{l1}(0)-\frac{ma\upsilon_{l1}(0)\upsilon_{l2}(-1)}{(a+x^*)^2} \\
&\quad -\frac{may^*\upsilon^3_{l1}(0)}{(a+x^*)^4}+\frac{ma\upsilon^2_{l1}(0)\upsilon_{l2}(-1)}{(a+x^*)^3}+\mathrm{h.o.t.},
\end{aligned}$$

$$K_{l2}^{*} = \frac{cma\upsilon_{l1}(0)\upsilon_{l2}(0)}{(a+x^{*})^{2}} - \frac{y^{*}cma\upsilon_{l1}^{2}(0)}{(a+x^{*})^{3}} + \frac{y^{*}cma\upsilon_{l1}^{3}(0)}{(a+x^{*})^{4}} - \frac{cma\upsilon_{l1}^{2}(0)\upsilon_{l2}(0)}{(a+x^{*})^{3}} + \text{h.o.t.}$$

Using Hassard's method, we calculate the following values:

$$\begin{aligned}
g_{20} &= \frac{2\tau_{l20}\overline{D}}{(a+x^{*})^{3}}\sum_{j=1}^{N}(\psi_{l}^{j})^{2}\overline{\psi_{l}^{j*}}[amc((a+x^{*})q_{l1}-y^{*})\overline{q_{l1}^{*}} \\
&\quad -k(a+x^{*})^{3}+amy^{*}-amq_{l1}(a+x^{*})\mathrm{e}^{-\mathrm{i}\omega_{0}\tau_{l20}}], \\
g_{11} &= \frac{\tau_{l20}\overline{D}}{(a+x^{*})^{3}}\sum_{j=1}^{N}\psi_{l}^{j}\overline{\psi_{l}^{j}\psi_{l}^{j*}}[amc((q_{l1}+\overline{q_{l1}})(a+x^{*})-2y^{*}) \\
&\quad \times\overline{q_{l1}^{*}}-2k(a+x^{*})^{3}+2amy^{*} \\
&\quad -am(a+x^{*})(q_{l1}\mathrm{e}^{-\mathrm{i}\omega_{0}\tau_{l20}}+\overline{q_{l1}}\mathrm{e}^{\mathrm{i}\omega_{0}\tau_{l20}})], \\
g_{02} &= \frac{2\tau_{l20}\overline{D}}{(a+x^{*})^{3}}\sum_{j=1}^{N}(\overline{\psi_{l}^{j}})^{2}\overline{\psi_{l}^{j*}}[amc((a+x^{*})\overline{q_{l1}}-y^{*})\overline{q_{l1}^{*}} \\
&\quad -k(a+x^{*})^{3}+amy^{*}-am\overline{q_{l1}}(a+x^{*})\mathrm{e}^{\mathrm{i}\omega_{0}\tau_{l20}}], \\
g_{21} &= -\frac{\tau_{l20}\overline{D}}{(a+x^{*})^{4}}\sum_{j=1}^{N}\overline{\psi_{l}^{j*}}[am(a+x^{*})^{2}W_{20}^{(2)}(-1) \\
&\quad -acm\overline{q_{l1}^{*}}(a+x^{*})^{2}W_{20}^{(2)}(0)+2am(a+x^{*})^{2}W_{11}^{(2)}(-1) \\
&\quad -2acm\overline{q_{l1}^{*}}(a+x^{*})^{2}W_{11}^{(2)}(0)] \\
&\quad +[am\overline{q_{l1}}\overline{\psi_{l}^{j}}(a+x^{*})^{2}\mathrm{e}^{\mathrm{i}\omega_{0}\tau_{l20}}+2(a+x^{*})(k(a+x^{*})^{3} \\
&\quad +amy^{*}(c\overline{q_{l1}^{*}}-1)-\frac{1}{2}acm\overline{q_{l1}}\overline{q_{l1}^{*}}\overline{\psi_{l}^{j}}(a+x^{*}))]W_{20}^{(1)}(0) \\
&\quad +(2amq_{l1}\psi_{l}^{j}(a+x^{*})^{2}\mathrm{e}^{-\mathrm{i}\omega_{0}\tau_{l20}}+4(a+x^{*})(k(a+x^{*})^{3} \\
&\quad +amy^{*}(c\overline{q_{l1}^{*}}-1)-\frac{1}{2}acmq_{l1}\psi_{l}^{j}\overline{q_{l1}^{*}}(a+x^{*})))W_{11}^{(1)}(0) \\
&\quad -2am(a+x^{*})(2q_{l1}\psi_{l}^{j}\mathrm{e}^{-\mathrm{i}\omega_{0}\tau_{l20}}+\overline{q_{l1}}\overline{\psi_{l}^{j}}\mathrm{e}^{\mathrm{i}\omega_{0}\tau_{l20}}) \\
&\quad +4ma[c\overline{q_{l1}^{*}}(a+x^{*})(q_{l1}\psi_{l}^{j} \\
&\quad +\frac{1}{2}\overline{q_{l1}}\overline{\psi_{l}^{j}})+\frac{3}{2}y^{*}(1-c\overline{q_{l1}^{*}})],
\end{aligned}$$

and

$$\begin{aligned}
W_{20}(\theta) &= \frac{\mathrm{i}g_{20}}{\omega_{0}\tau_{l20}}q(0)\mathrm{e}^{\mathrm{i}\omega_{0}\tau_{l20}\theta}+\frac{\mathrm{i}\overline{g}_{02}}{3\omega_{0}\tau_{l20}}\overline{q}(0)\mathrm{e}^{-\mathrm{i}\omega_{0}\tau_{l20}\theta} \\
&\quad +E_{2}\mathrm{e}^{2\mathrm{i}\omega_{0}\tau_{l20}\theta}, \\
W_{11}(\theta) &= -\frac{\mathrm{i}g_{11}}{\omega_{0}\tau_{l20}}q(0)\mathrm{e}^{\mathrm{i}\omega_{0}\tau_{l20}\theta} \\
&\quad +\frac{\mathrm{i}\overline{g}_{11}}{\omega_{0}\tau_{l20}}\overline{q}(0)\mathrm{e}^{-\mathrm{i}\omega_{0}\tau_{l20}\theta}+E_{1},
\end{aligned}$$

further calculate the key bifurcation parameters.

(i) The direction of the Hopf bifurcation $\mu_2 = -\frac{\mathrm{Re}\{c_1(0)\}}{\mathrm{Re}\{\lambda'(\tau_{l20})\}}$. Precisely, in the case where $\mathrm{Re}\{\lambda'(\tau_{l20})\}>0$, if $\mu_2>0$ (alternatively, $\mu_2<0$), the Hopf bifurcation is supercritical (subcritical correspondingly), and the periodic solution comes into existence for $\tau_2>\tau_{l20}$ (respectively $\tau_2<\tau_{l20}$). If $\mathrm{Re}\{\lambda'(\tau_{l20})\}<0$, however, the bifurcating periodic solutions will be in the opposite direction.

(ii) The stability of the bifurcated periodic solutions $\beta_2 = 2\mathrm{Re}\{c_1(0)\}$. To be exact, the bifurcation periodic solutions possess stability when $\beta_2<0$; conversely, they lack stability when $\beta_2>0$.

(iii) The period of the bifurcated periodic solutions $T_2 = -\frac{\mathrm{Im}\{c_1(0)\}+\mu_2\mathrm{Im}\{\lambda'(\tau_{l20})\}}{\omega_0\tau_{l20}}$. More precisely, the period experiences an increment when $T_2>0$; in contrast, it undergoes a decrement when $T_2<0$, where

$$c_1(0) = \frac{i}{2\omega_0\tau_{l20}}\left(g_{20}g_{11}-2|g_{11}|^2-\frac{1}{3}|g_{02}|^2\right)+\frac{g_{21}}{2}.$$

4. Simulation

To verify the theoretical results, we consider the following specific form of system (3):

$$\begin{cases}
\dfrac{\mathrm{d}x_i}{\mathrm{d}t} = 1.2x_i(t-\tau_1)-1.2x_i^2-\dfrac{2.5x_iy_i(t-\tau_2)}{0.7+x_i}+k_1\sum_{j=1}^{N}L_{ij}x_j, \\
\dfrac{\mathrm{d}y_i}{\mathrm{d}t} = \dfrac{2.5x_iy_i}{0.7+x_i}-1.1y_i+k_2\sum_{j=1}^{N}L_{ij}y_j.
\end{cases} \tag{27}$$

The positive equilibrium of system (27) is $E^{*} = (0.55, 0.27)$.

For numerical illustration, we focus on the Laplacian mode $\Lambda_1 = 0$. Here, $\Lambda_1 = 0$ is considered purely as a Laplacian mode in the modal stability analysis, rather than as a criterion for network connectivity. The purpose of this section is twofold: first, to verify the stability-switching and Hopf bifurcation results obtained in Sections 2 and 3; second, to illustrate representative dynamical behaviors of the networked system for different values of the link probability p.

For the mode $\Lambda_1 = 0$, Eq. (5) reduces to

$$\lambda^{2}+1.6224\lambda-1.2\lambda\mathrm{e}^{-\lambda\tau_1}+0.3326\mathrm{e}^{-\lambda\tau_2} = 0. \tag{28}$$

When $\tau_1=\tau_2=0$, the roots of Eq. (28) are $-0.2112\pm 0.5367\mathrm{i}$, which implies that the positive equilibrium E^{*} is asymptotically stable.

When at least one of τ_1 and τ_2 is nonzero, Lemma 1 shows that $\lambda = \mathrm{i}\omega$ is a solution of Eq. (28) if and only if $\omega\in(0.1175, 0.6198)$. Accordingly, the admissible frequency interval is obtained from the functions $F_{11}(\omega)$, $F_{12}(\omega)$, and $F_{13}(\omega)$, as shown in Fig. 1(a). Based on Theorem 2, the corresponding stability-switching curve T_1 in the (τ_1,τ_2)-plane is plotted in Fig. 1(b), and the region enclosed by the coordinate axes and T_1 gives the asymptotically stable region of the positive equilibrium E^{*}.

To further validate the theoretical prediction, we directly compute the characteristic roots of Eq. (28) at several representative points in the (τ_1,τ_2)-plane. We select one point inside the stable region, one point near the switching curve, and one point in the unstable region. The corresponding rightmost

roots confirm that the maximum real part is negative in the stable region, close to zero near the switching curve, and positive in the unstable region. Hence, the direct root computation is consistent with the prediction of Theorem 2, as shown in Table 1.

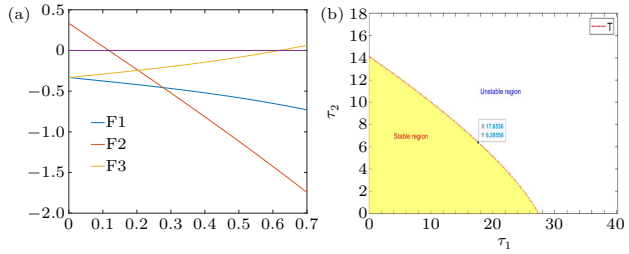


Fig. 1. (a) The functions $F_{11}(\omega)$, $F_{12}(\omega)$, and $F_{13}(\omega)$ for the mode $\Lambda_1 = 0$. The admissible frequency interval is $\omega \in (0.1175, 0.6198)$. (b) The stability-switching curve T_1 in the (τ_1, τ_2)-plane. The shaded region T_1^0 corresponds to the asymptotically stable region of the positive equilibrium E^*.

Figure 2 displays three representative dynamical regimes corresponding to the above parameter choices. For $(\tau_1, \tau_2) = (9, 5)$, the solution converges to the positive equilibrium E^*, which agrees with the stability prediction. For $(\tau_1, \tau_2) = (17.6536, 6.38558)$, the trajectory exhibits periodic oscillations near the stability-switching boundary, indicating the onset of Hopf bifurcation. For $(\tau_1, \tau_2) = (29, 10)$, the equilibrium loses stability, and the solution exhibits more complex oscillatory behavior.

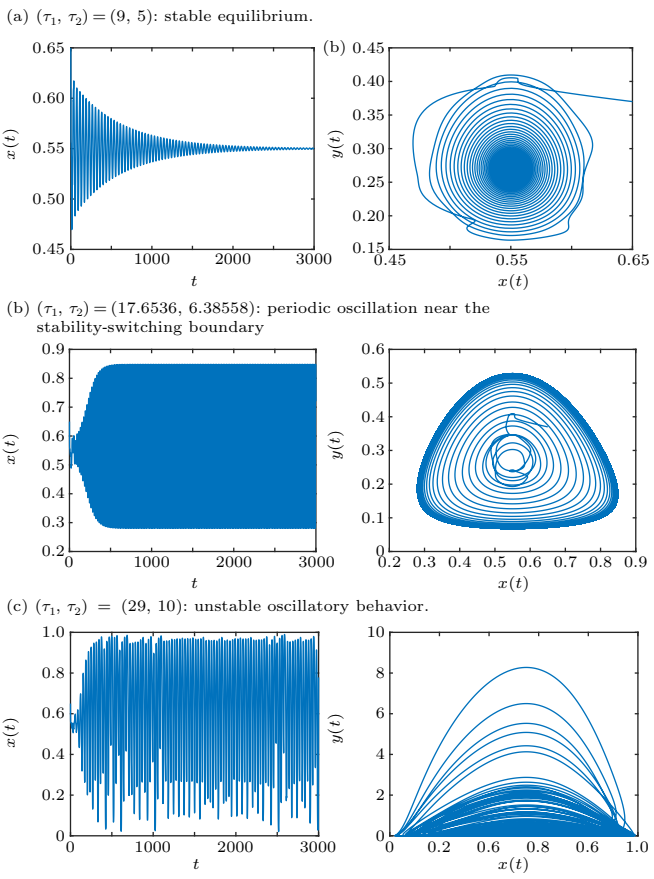


Fig. 2. Representative dynamics of system (27) for the mode $\Lambda_1 = 0$. Left column: time series of the prey density $x(t)$. Right column: phase portraits in the $(x(t), y(t))$-plane.

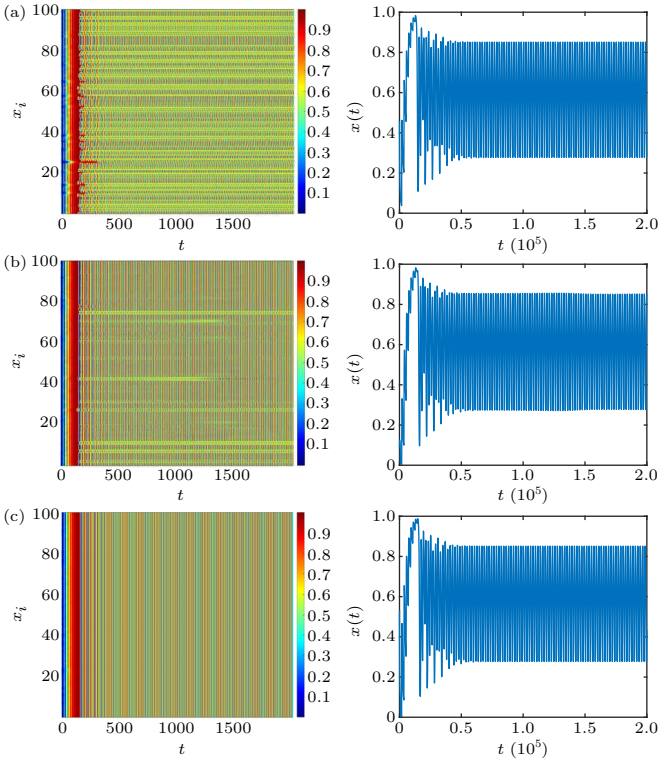


Fig. 3. Numerical solutions of system (27) for three representative values of the link probability p: (a) $p = 0$, (b) $p = 0.03$, and (c) $p = 0.07$. This figure illustrates how the temporal behavior changes as the network coupling becomes stronger.

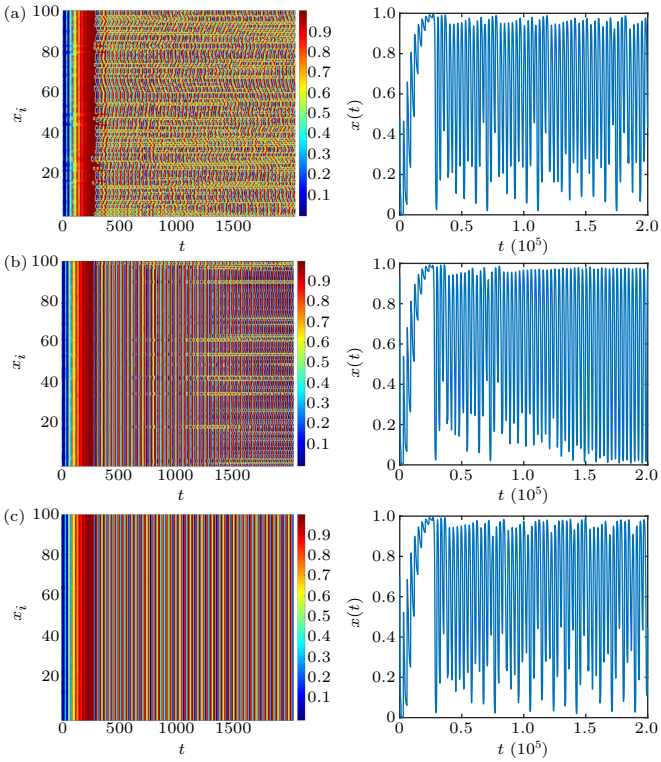


Fig. 4. Further numerical illustrations of system (27) for three representative values of the link probability p: (a) $p = 0$, (b) $p = 0.03$, and (c) $p = 0.07$. The results show the corresponding network-level dynamical patterns under different coupling strengths.

Next, we illustrate how different values of the link probability p affect the observed dynamical behavior of the networked system. Here, p is used only as a numerical parameter

Table 1. Direct numerical validation of the characteristic roots of Eq. (28) at representative points.

Point	(τ_1,τ_2)	Rightmost roots	$\max\Re(\lambda)$	Stability
A	$(9,5)$	$-0.001614\pm0.164215\mathrm{i}$	-0.001614	stable
B	$(17.6536, 6.38558)$	$0.000731\pm0.312401\mathrm{i}$	0.000731	unstable (near Hopf boundary)
C	$(29,10)$	$0.028545\pm0.187663\mathrm{i}$	0.028545	unstable

in the random network construction, and the following simulations are intended to provide qualitative illustrations rather than additional theoretical conclusions.

We consider three representative cases: $p=0$, $p=0.03$, and $p=0.07$.

When $p=0$, the nodes are effectively isolated from one another, and the dynamics at different nodes evolve independently. In this case, the network exhibits weak coherence, and the temporal behaviors are mainly governed by the local node dynamics.

When $p=0.03$, the coupling between nodes is present but remains relatively weak. As a result, interactions among neighboring nodes become visible, and the solutions exhibit partial coherence together with noticeable spatial heterogeneity.

When $p=0.07$, the coupling effect becomes stronger, and the collective dynamics become more coherent across the network. The simulations indicate that stronger coupling tends to suppress disorder and promote more coherent collective behavior.

Figures 3 and 4 present the corresponding numerical solutions for these three values of p. These results show that, under the same local parameters, varying the network link probability may significantly influence the observed temporal and spatiotemporal patterns of the coupled predation system.

5. Conclusion

In this paper, we investigated a two-delay predation system with diffusion and network coupling. By combining the Laplacian-mode decomposition with the Kronecker-product formulation, we reduced the stability analysis of the high-dimensional networked system to a family of mode-dependent characteristic equations. On this basis, we derived the corresponding stability-switching curves in the (τ_1,τ_2)-plane and obtained sufficient criteria for the stability of the positive equilibrium.

Furthermore, by employing the Hassard method and center-manifold reduction, we analyzed the Hopf bifurcation generated at the critical delay values and characterized the direction of bifurcation, the stability of the bifurcating periodic solutions, and the variation of their periods. These results clarify how the interplay between the two delays influences the local dynamics near the positive equilibrium.

The numerical examples support the theoretical analysis. In particular, the stability-switching curves predicted by the characteristic equation are consistent with the simulated dynamical behaviors observed at representative parameter points. The simulations further illustrate typical temporal and spatiotemporal patterns under network coupling.

Overall, the present study establishes a tractable analytical approach for studying delay-induced stability switching and Hopf bifurcation in predation systems with diffusion and network coupling. The framework developed here may also be useful for analyzing other delayed networked biological models with similar coupling mechanisms.

Future work may consider extending the present setting to more general ecological systems, such as models with multiple interacting species, heterogeneous delays, or stochastic perturbations, in order to further understand the influence of complex ecological factors on the stability and oscillatory behavior of networked population systems.

Acknowledgements

This work is supported by the Key Scientific Research Project of Colleges and Universities in Henan Province(Grant No. 24B110017) and the Natural Science Foundation of Henan Province(Grant No. 242300420661).

References

[1] Hsu S B and Huang T W 1995 *SIAM J. Appl. Math.* **55** 3
[2] Freedman H I 1980 *Deterministic Mathematical Models in Population Ecodogy* (New York: Marcel Dekker Press)
[3] Lotka A J 1925 *Elements of physical biology* (Baltimore: Williams and Wilkins Press)
[4] Volterra V 1926 *Nature* **118** 2972
[5] Smith H 2010 *An Introduction to Delay Differiential Equation with Applications to the Life Sciences* (New York: Springer Press)
[6] Xia Y, Huang X, Chen F and Chen L 2024 *J. Biol. Syst.* **32** 02
[7] Duan D, Niu B, Wei J and Yuan Y 2024 *Eur. J. Appl. Math.* **35** 5
[8] Shu R, Chen W and Xiao J H 2019 *Acta Phys. Sin.* **68** 18
[9] Wang J H , Xu Y L , Zhang J and Yang D D 2018 *Chin. Phys. B* **27** 4
[10] Miao L and Zhu L 2024 *Commun. Nonlinear Sci. Numer. Simul.* **135** 108045
[11] Lv Y 2025 *Math. Methods Appl. Sci.* **36** 04
[12] Gupta R P, Tiwari S and Kumar A 2025 *Math. Comput. Simul.* **229**
[13] Suriguga, Jia Y, Wang J and Li Y 2024 *Results Phys.* **61** 107792
[14] Wang H, Dai Y and Zhou S 2024 *Math. Methods Appl. Sci.* **48** 2
[15] Kumar B and Sinha R K 2025 *J. Appl. Math. Comput.* **71** 1
[16] Shi R and Hu Z 2025 *Int. J. Comput. Math.* **102** 9
[17] Gou W, Jin Z and Wang H 2023 *J. Differ. Equ.* **346**
[18] Jiao X, Liu L and Yu X 2025 *Math. Comput. Simul.* **228**
[19] Zhou X, Wang X and Zhang G 2025 *Appl. Math. Lett.* **160** 109334
[20] Han Q S , Chen D Y and Zhang H 2017 *Chin. Phys. B* **26** 12
[21] Gou W, Song Y and Jin Z 2023 *SIAM J. Appl. Dyn. Syst.* **22** 2
[22] Yuan C and Yin G 2010 *J. Math. Anal. Appl.* **368** 1
[23] Singh A, Kumar A, Gupta A and Dubey B 2025 *Int. J. Bifurcation Chaos* **35** 2550018
[24] Hou Y and Ding Y 2024 *Nonlinear Dyn.* **112** 12
[25] Lu H and Guo Y 2024 *Int. J. Bifurcation Chaos* **34** 2450155
[26] Alfifi H Y 2024 *Appl. Math. Comput.* **474** 128684
[27] Yang W J, Zheng Q Q and Shen J W 2024 *Int. J. Biomath.* **17** 2350014
[28] Yang P and Lin Y 2022 *J. Appl. Anal. Comput.* **12** 03
[29] Hassard B D, Kazarinoff N D and Wan Y H 1981 *Theory and Applications of Hopf Bifurcation* (Cambridge: Cambridge University Press)